A Combined Quantum Chemistry and RRKM Calculation Predicts the $O(^1D) + C_2H_6$ Reaction Can Produce Water Molecule in a Collision-Free Crossed Molecular Beam Environment

Ying-Chieh Sun,*,† I-Ting Wang,† Thanh Lam Nguyen,‡ Hsiu-Feng Lu,† Xueming Yang,‡,§ and Alexander M. Mebel*,‡

Department of Chemistry, National Taiwan Normal University, 88 Tingchow Road Sec. 4, Taipei 11718, Taiwan, Republic of China, Institute of Atomic and Molecular Sciences, Academia Sinica, Taipei, Taiwan, Republic of China, and Chemistry Department, National Tsing Hua University, Hsinchu, Taiwan, Republic of China

Received: November 11, 2002; In Final Form: June 26, 2003

The $O(^1D) + C_2H_6$ reaction has been studied using a combined quantum chemistry and RRKM calculation to find the rate constants for the elementary reaction channels. The calculations of the relative branching ratios for various products formed through the insertion mechanism have been carried out. The calculations gave 60, 8, 4, 1, and 27% for the CH_3, OH, H, H_2, and H_2O formation channels, respectively. These calculated results for the first four species are in good agreement with the available experimental results of 70, 25, 3, and 2%, while water molecules were not detected in the experiments. It is noted that the calculations underestimated the branching ratio for OH formation channel and predicted that a large quantity of water molecules would be formed. In addition to the calculation for the insertion mechanism, the abstraction mechanism pathway via a weak $O-C_2H_6$ complex has been examined as well. The calculation gave a low energy barrier of 2.2 kcal/mol for this mechanism, supporting the conclusion that OH formation through this abstraction channel is not negligible. The contribution by this mechanism should compensate the underestimation of the calculated value for the OH product shown above, compared with the experimental result obtained when only insertion is considered in the computation. Furthermore, the result of the large branching ratio for H_2O formation shows that H_2O is an important minor product of the $O(^1D) + C_2H_6$ reaction. The water molecule is formed mainly by the OH and a β H, suggesting that H_2O will be a non-negligible product in the reactions of $O(^1D)$ + simple alkane derivatives which have a β H. Formation of water molecules in the molecular beam collision-free environment can be verified in future experiments. Reaction rates of all elementary reactions to produce the various products described above are reported and discussed.

I. Introduction

The reactions of small organic molecules with an oxygen atom have been an interesting subject for experimental and theoretical studies during the past few decades because of their importance in combustion and atmospheric chemistry.[1−21] Recent advances in experimental investigations for understanding the dynamics of elementary reactions of gas molecules using crossed molecular beams have provided tremendous insight into reaction dynamics in the gas phase for various reactant species.[1−4,7−13,20,21] The latest developments in the universal molecular beam apparatus provide a powerful tool for investigating the complete reaction dynamics in great detail on a state-to-state level.[7,9,17,20−22] The reaction dynamics of various small alkane molecules and their derivatives with an oxygen atom were very revealing.[7,9,17,20−22] Recently, a series of investigations of O + simple alkane reactions were carried out to unravel their detailed dynamics. An oxygen atom can insert into a C−H bond to form an alcohol, and then the follow-up reactions of this energized alcohol molecule proceed, or it can take one hydrogen atom away to form the OH radical directly, termed an abstraction mechanism. The OH radical formed by the latter mechanism is likely to be produced via a short-lived complex, while the insertion mechanism involves a long-lived complex.[20,21] The experimental investigations revealed that the abstraction mechanism is not significant in the $O(^1D) + CH_4$ reaction but, for $O(^1D)$ + larger simple alkanes, this mechanism has a non-negligible contribution in producing the OH radical.[7,9,20,21] This is supported by the results of the product distribution in the observed scattering angle in recent investigations using the universal crossed beam method.[7,9,20,21] Nevertheless, the insertion mechanism is the dominant reaction pathway for these reactions,[20,21] as found for many other reactions.[10,23] Thus, the reaction channel through the insertion mechanism should mainly account for the product branching ratio observed in the experiments. In addition, for larger alkane molecules, like C_2H_6, for example, due to steric hindrance and the bond number ratio of 6:1 for C−H and C−C bonds in ethane, the oxygen atom is much less likely to insert into the C−C bond, compared with the C−H bond. Recent theoretical calculations also showed that the insertion into the C−C bond is forbidden.[24] Thus, the reaction of $O(^1D) + C_2H_6$ will mainly go through the reaction channel to first form energized ethanol. Previous investigations showed that the formations of $C_2H_4 + H_2O$ and $CH_3 + CH_2$-

* Corresponding authors.
† National Taiwan Normal University.
‡ Academia Sinica.
§ National Tsing Hua University.

10.1021/jp027439t CCC: $25.00
Published on Web 08/16/2003

OH are two dominant decomposition channels at high temperatures.[24−26] The detailed dynamics of this reaction, including energy partitioning, product branching ratios, and reaction mechanisms after collision, were uncovered in great detail using the universal crossed molecular beam method.[20,21]

In addition to the experimental investigations, theoretical calculations based on the combined quantum chemistry and RRKM method have provided complementary calculated results and predictions for understanding the reaction kinetics of a number of reactions involving various molecules.[5,6,15,28,29] For the $O(^1D)$ + simple alkane molecules, theoretical investigations of the $O(^1D) + CH_4$ reaction were carried out.[28,29] In addition to the examination of this reaction in a vacuum,[29] the temperature dependence of the reaction rate constants covering the temperature range of 1000−3000 K at low and high pressures were reported.[28] Earlier calculations for examining the unimolecular decomposition of ethanol showed that a nonnegligible amount of water can form in addition to the other two major products, CH_3 and OH radicals.[1,3] Calculation for $O(^1D)$ + cyclopropane was also carried out.[31] Recently, Lin and co-workers reported an RRKM study investigating thermal decomposition of ethanol.[32] The calculated results are in good agreement with experimental results.[1,3,28,31] Theoretical examinations along this line have revealed much of the details of the kinetics of $O(^1D)$ + simple alkanes.[1,3,28,30] In the present study, in parallel with the experimental investigation of the $O(^1D) + C_2H_6$ reaction in the secondary-collision-free crossed molecular beam environment with a collision energy of 8 kcal/mol,[20,21] we report the results of the reaction rates for elementary steps of the $O(^1D) + C_2H_6$ reaction, calculated using quantum chemistry combined with the RRKM theory. In the experiments, the O atom source contains both $O(^1D)$ and $O(^3P)$ atoms. It has been shown that $O(^1D)$ is much more reactive with the alkane molecules than the $O(^3P)$ atoms. The reaction products of $O + C_2H_6$ come mainly from the $O(^1D) + C_2H_6$ reaction.[20] Thus, the present study focuses only on the $O(^1D) + C_2H_6$ calculation. As described above, the insertion mechanism is the dominant reaction pathway compared with the abstraction mechanism for the reaction of $O(^1D) + C_2H_6$. Hence, similar to previous theoretical investigations for other reactions[5,6,30,31] using the combined quantum chemistry calculation and RRKM approach, the present calculation also focuses on examining this insertion channel. In the experimental investigations for O + ethane,[20,21] the observed relative product branching ratios for CH_3, OH, H, and H_2 are 70, 25, 3, and 2%, respectively. The present calculated product branching ratios are in good agreement with available experimental results. Interestingly, the calculation shows a significant amount of water formed in this reaction, which was not observed in the experiments.[20,21]

The following sections are organized as follows. Section II describes the RRKM theory and quantum chemistry calculation used in the present study. The results and discussion are given in section III. Concluding remarks are given in section IV.

II. Methods

The theory of and methods to compute reaction rates have been described in the literature.[5,6,30] Briefly, we consider a unimolecular reaction,

$$R^* \xrightarrow{k} R^{\neq} \rightarrow P \qquad (1)$$

where R^* is the energized reactant, $R^{\neq}$ is the activated reacting complex, and P is the product. By assuming that this reaction is statistical,[33] the rate constant k is given, on the basis of the RRKM theory, by

$$k(E) = \frac{\sigma}{h}\frac{W(E - E^{\neq})}{\rho(E)} \qquad (2)$$

where σ is the symmetry number and h is the Planck constant. $W(E - E^{\neq})$ is the number of states for the activated reacting complex at the energy difference between the total energy E and the reaction barrier, $E^{\neq}$. $\rho(E)$ is the density of state of the energized reactant at total energy E. These two quantities can be found by using the saddle point method.[33] In these equations, the electronic ground-state energy, the vibrational frequencies of the calculated species at the reactant and the transition state (TS), and the total available energy E are needed as inputs. The calculated $W(E - E^{\neq})$ and $\rho(E)$ are used in turn to calculate the rate constant in eq 2 for the elementary reaction being examined. For a reaction without an energy barrier, for instance, the breaking of the C−C (or C−O, C−H, O−H) bond in the activated ethanol, the rate constant is determined by the criterion according to the microcanonail variational transition state theory (MVTST):[33,34]

$$\frac{\partial W(E - E^{\neq})}{\partial R_C} = 0 \qquad (3)$$

For the C−C bond cleavage case, R_C is the distance between two C atoms. The number of states $W(E - E^{\neq})$ along this coordinate was calculated, and the R_C point which satisfies the criterion of eq 3 is considered to be the variational TS point for this bond-breaking barrierless reaction (see the third and fourth paragraphs of this section for detailed description). With these data described above in hand, the rate constants for all elementary reactions can be obtained. It should be noted that excellent progress has been made in the development of reaction path calculation in order to obtain an accurate rate constant (for example, refs 35 and 36) for a reaction proceeding on a multidimensional potential surface. In the present calculation (see the third and fourth paragraphs of this section for details), we simply varied the distance of the C−C bond at some fixed bond distances in order to find the variational point and the resulting rate constant k.

To find the electronic ground-state energy and vibrational frequencies of the calculated species, the Gaussian 98 program[37] was used in the present study. The geometry of equilibrium structures and transition states of various species were optimized by employing the hybrid density functional B3LYP method with the 6-311G(d,p) basis set. The optimized structures are shown in Figure 1. Vibrational frequencies of the examined species were obtained at this B3LYP/6-311G(d,p) level as well. To obtain more accurate energies, a single-point calculation with the CCSD(T) method and the large 6-311+G(3df,2p) basis set for all optimized structures was carried out. A similar CCSD(T)/B3LYP approach has been used and demonstrated to have a sufficient accuracy in calculation of energy for the species examined.[15,30,31] The calculated energies and the zero-point energies (ZPE) of the reactant, product species, and identified TS on the potential energy surface are listed in Table 1. The calculated vibrational frequencies are listed in Table 2. To account for the change of the number of paired and unpaired electrons for product species of two radicals, e.g., $C_2H_5O + H$ using the CCSD(T)/6-311+G(3df,2p)//B3LYP/6-311G(d,p) computational procedure, a "higher level correction (HLC)"[38] was included in energy calculation. Finally, the ZPE was added to

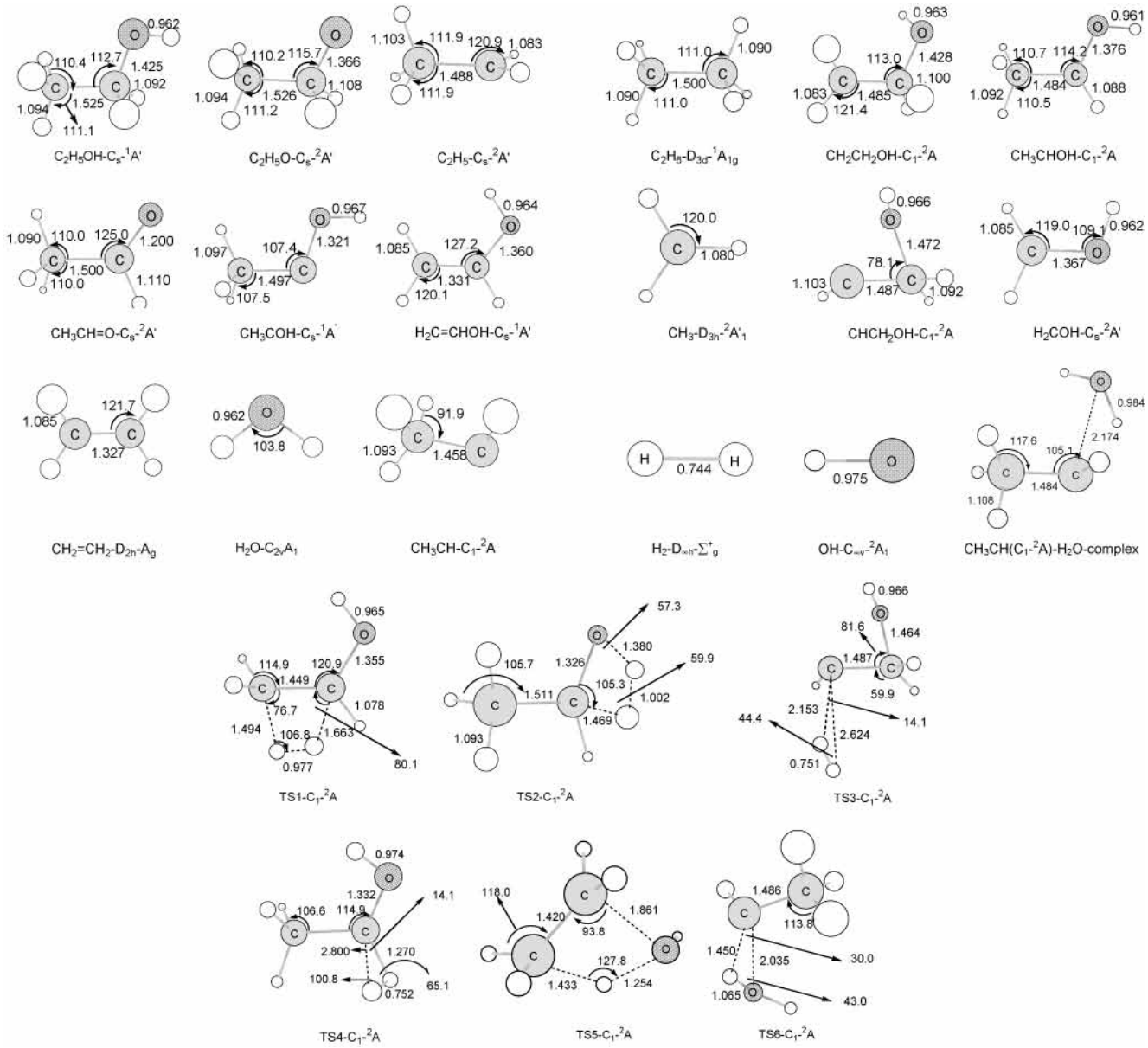

Figure 1. Optimized structure of the considered molecular species with symmetry labeled. Distance values between atoms are given in angstroms. Angles are given in degrees.

the calculated B3LYP/6-311G(d,p), CCSD(T)/6-311+G(3df,-2p), and CCSD(T)/6-311+G(3df,2p) + HLC energies to give the final calculated energy of the considered molecular species, listed in kilocalories per mole in Table 3. The CCSD(T)/6-311G-(3df,2p) + HLC energies of these species are shown in the energy profile of this $O(^1D) + C_2H_6$ reaction in Figure 2 and used for calculation of the number and density of states, $W(E - E^{\neq})$ and $\rho(E)$, in eq 2, respectively.

For those bond-breaking, energy-barrierless reaction channels, the TS were identified by calculating the number of states, $W(E - E^{\neq})$, along the breaking bond coordinate as described above. For example, for the C−C bond-breaking case, the $W(E - E^{\neq})$ calculation started with the optimized reactant C_2H_5OH structure, except that the C−C bond was lengthened to an estimated bond distance of 2.0 Å according to experience from previous calculations.[30] The potential energy surface was then scanned at the UB3LYP/6-311G(d,p) level along the bond distance, which was taken as the length of the breaking bond. To do that, we carried out partial geometry optimization for a series of fixed values of this bond distance, while all other geometric parameters were optimized. For the partially optimized geometric structures, we performed calculations of $3N - 7$ vibrational frequencies with bond distance fixed at selected bond distances.[39] As a single C−C or C−H bond breaks, the character of the wave function changes from a closed-shell singlet to an open-shell singlet since both decomposition products have doublet wave functions. At large values of the bond distance, where variational TS's are usually found, the wave function has an open-shell character. Therefore, we calculated the open-shell singlet energies at the unrestricted UB3LYP level.

To obtain an open-shell singlet wave function, we first carried out single-point calculations of the triplet state wave function, and the latter was used as an initial guess for the open-shell singlet calculations. It should be noted that this computationally affordable unrestricted UB3LYP approach has been shown to provide a reasonable accuracy for the energies and molecular parameters of open-shell singlet species.[37] Also, the UB3LYP energies and vibrational frequencies change smoothly, without oscillations, along the bond distance for all variational TS's considered in this work. The calculated energy plus ZPE is considered to be the energy of this species at this structure. These calculated energies and vibrational frequencies were then

TABLE 1: Calculated Energy of Molecular Species at the Levels of B3LPY/6-311G(d,p) and CCSD/6-311+G(3df,2p), and Their Zero-Point Energy (ZPE) Obtained Using B3LYP/6-311G(d,p)

species	B3LYP/ 6-311G(d,p) (au)	CCSD(T)/ 6-311+G(3df,2p) (au)	ZPE[g] (kcal/mol)
$O(^1D)+C_2H_6(D_{3d}\text{-}^1A_{1g})$	−154.83951	−154.55584	46.67
$C_2H_5OH(C_s\text{-}^1A')$	−155.08848	−154.78906	50.12
$C_2H_5O(C_s\text{-}^2A') + H$	−154.91923	−154.61359	40.24
$CH_2CH_2OH(C_1\text{-}^2A) + H$	−154.91745	−154.61759	40.82
$C_2H_5(C_s\text{-}^2A') + OH(C_{\infty v}\text{-}^2A_1)$	−154.93818	−154.63241	42.32
$CH_3CHOH(C_1\text{-}^2A) + H$	−154.93137	−154.62949	41.29
$H_2COH(C_s\text{-}^2A') + CH_3(D_{3h}\text{-}^2A'_1)$	−154.94936	−154.64329	41.95
$CH_3CH(C_1\text{-}^1A)-H_2O(C_{2v}\text{-}^1A_1)$ complex	−154.95673	−154.65256	45.62
$CHCH_2OH(C_1\text{-}^1A) + H_2(D_{\infty h}\text{-}^1\Sigma^+_g)$	−154.90255	−154.60372	40.64
$CH_3COH(C_s\text{-}^1A') + H_2(D_{\infty h}\text{-}^1\Sigma^+_g)$	−154.97396	−154.67273	40.78
$H_2C{=}CHOH(C_s\text{-}^1A') + H_2(D_{\infty h}\text{-}^1\Sigma^+_g)$	−155.03926	−154.73702	41.76
$CH_3CH{=}O(C_s\text{-}^1A') + H_2(D_{\infty h}\text{-}^1\Sigma^+_g)$	−155.05643	−154.75364	40.96
$CH_2{=}CH_2(D_{2h}\text{-}^1A_g) + H_2O(C_{2v}\text{-}^1A_1)$	−155.06143	−154.76492	45.26
$CH_3CH\ (C_1\text{-}^1A) + H_2O(C_{2v}\text{-}^1A_1)$	−154.93917	−154.64349	42.54
TS1[a]	−154.91695	−154.61220	43.89
TS2[b]	−154.94525	−154.64234	44.05
TS3[c]	−154.90365	−154.60432	42.17
TS4[d]	−154.94706	−154.64120	43.35
TS5[e]	−154.97988	−154.67376	44.83
TS6[f]	−154.95595	−154.64998	44.76

[a] $C_2H_5OH \rightarrow H_2C{=}CHOH + H_2$. [b] $C_2H_5OH \rightarrow CH_3CH{=}O + H_2$. [c] $C_2H_5OH \rightarrow CHCH_2OH + H_2$. [d] $C_2H_5OH \rightarrow CH_3COH + H_2$. [e] $C_2H_5OH \rightarrow CH_2{=}CH_2 + H_2O$. [f] $C_2H_5OH \rightarrow CH_3CH + H_2O$. [g] Zero-point energy.

TABLE 2: Vibrational Frequencies of Molecular Species Using B3LYP/6-311G(d,p) Level (in cm^{-1})

species	vibrational frequencies (cm^{-1})
$C_2H_5OH(C_s\text{-}^1A')$	252.1, 288.7, 418.4, 827.2, 902.9, 1035.4, 1108.2, 1180.7, 1278.6, 1302.6, 1406.9, 1461.9, 1481.1, 1503.2, 1531.3, 2965.0, 2988.9, 3033.9, 3101.3, 3105.4, 3839.3
$C_2H_6(D_{3d}\text{-}^1A_{1g})$	305.9, 827.2, 827.6, 997.8, 1219.2, 1219.5, 1410.0, 1425.4, 1504.7, 1504.9, 1507.3, 1507.8, 3025.5, 3025.9, 3071.6, 3071.7, 3097.0, 3097.1
$C_2H_5O(C_s\text{-}^2A')$	124.2, 286.1, 433.1, 869.6, 887.4, 1068.8, 1098.9, 1240.9, 1342.4, 1390.2, 1411.8, 1485.3, 1496.6, 2888.1, 2891.8, 3030.0, 3096.8, 3106.6
$CH_2CH_2OH(C_1\text{-}^2A)$	204.0, 367.1, 427.8, 546.8, 829.1, 952.5, 1082.3, 1119.1, 1185.6, 1366.6, 1403.2, 1450.9, 1485.5, 2961.3, 2981.0, 3134.7, 3243.5, 3814.8
$C_2H_5(C_s\text{-}^2A')$	108.4, 477.8, 813.1, 979.9, 1062.3, 1191.6, 1400.5, 1465.1, 1482.6, 1482.8, 2942.8, 3034.8, 3078.1, 3138.6, 3238.4
$OH(C_{\infty v}\text{-}^2A_1)$	3704.6
$CH_3CHOH(C_1\text{-}^2A)$	181.7, 365.1, 410.0, 581.1, 930.3, 1024.2, 1060.2, 1207.8, 1279.7, 1395.1, 1449.0, 1465.4, 1491.6, 2943.7, 3040.8, 3094.4, 3115.2, 3844.9
$H_2COH(C_s\text{-}^2A')$	439.5, 586.6, 1061.4, 1207.1, 1366.9, 1488.0, 3111.6, 3256.0, 3840.3
$CH_3(D_{3h}\text{-}^2A'_1)$	504.5, 1403.0, 1403.0, 3105.1, 3284.2, 3284.2
CH_3CH-H_2O complex	129.8, 212.7, 267.7, 287.0, 370.2, 535.5, 758.8, 862.8, 953.4, 1092.6, 1269.9, 1345.5, 1418.6, 1503.4, 1628.4, 2941.6, 2986.6, 3005.4, 3062.6, 3452.2, 3830.3
$CHCH_2OH(C_1\text{-}^1A)$	305.5, 484.3, 875.7, 896.4, 965.9, 1045.1, 1104.9, 1266.2, 1277.3, 1322.2, 1534.9, 2975.9, 3046.8, 3106.7, 3804.3
$CH_3COH(C_s\text{-}^1A')$	107.7, 510.3, 737.5, 912.3, 979.1, 1050.9, 1293.1, 1339.5, 1374.6, 1445.4, 1465.3, 2985.8, 3066.5, 3074.0, 3763.6
$H_2C{=}CHOH(C_s\text{-}^1A')$	476.2, 491.4, 714.5, 823.8, 961.0, 998.3, 1126.5, 1327.0, 1359.5, 1448.5, 1703.2, 3138.8, 3184.2, 3238.0, 3803.2
$CH_3CH{=}O(C_s\text{-}^1A')$	159.7, 507.9, 776.7, 881.8, 1125.2, 1135.4, 1374.2, 1425.9, 1460.2, 1471.0, 1825.1, 2855.3, 3021.7, 3077.5, 3136.4
$H_2(D_{\infty h}\text{-}^1\Sigma^+_g)$	4418.9
$CH_2{=}CH_2(D_{2h}\text{-}^1A_g)$	834.4, 972.5, 973.1, 1066.4, 1238.7, 1379.6, 1471.9, 1692.0, 3122.5, 3137.6, 3194.0, 3222.4
$CH_3CH(C_1\text{-}^2A)$	477.0, 614.6, 959.2, 1118.8, 1265.4, 1304.0, 1349.7, 1512.8, 2830.2, 2902.4, 2988.3, 3079.5
$H_2O(C_{2v}\text{-}^1A_1)$	1638.8, 3809.7, 3906.6
$O-C_2H_6(C_s\text{-}^1A'')$[a]	22.0, 35.3, 326.7, 866.7, 875.0, 1051.6, 1291.4, 1314.0, 1490.6, 1521.9, 1589.4, 1593.6, 1594.7, 1599.3, 2960.9, 2971.4, 3157.7, 3164.7, 3225.0, 3250.8
TS1[b]	1759.0 i, 311.2, 490.2, 547.1, 639.2, 933.8, 953.2, 1006.2, 1075.6, 1180.6, 1260.0, 1318.0, 1386.6, 1429.2, 1512.2, 1570.5, 1897.0, 2960.9, 3184.1, 3240.5, 3803.0
TS2[c]	2205.4 i, 254.0, 438.0, 616.3, 819.1, 965.5, 1039.1, 1152.7, 1254.0, 1368.1, 1387.6, 1411.7, 1466.6, 1483.4, 1903.6, 2178.3, 2923.8, 3028.0, 3097.3, 3136.3
TS3[d]	96.1 i, 122.1, 176.2, 305.5, 413.6, 442.4, 499.9, 865.9, 907.8, 966.3, 1050.7, 1115.3, 1266.3, 1286.9, 1334.7, 1535.8, 2985.3, 3045.8, 3103.6, 3800.2, 4272.3
TS4[e]	1019.4 i, 282.3, 463.6, 534.8, 598.8, 690.8, 922.1, 990.7, 1061.3, 1207.6, 1311.5, 1350.2, 1402.3, 1464.6, 1481.4, 1645.6, 2212.6, 2951.9, 3046.4, 3122.6, 3582.4
TS5[f]	2008.0 i, 346.8, 419.4, 544.3, 602.3, 742.3, 830.1, 837.9, 1031.6, 1125.1, 1227.3, 1234.0, 1413.5, 1460.7, 1521.3, 1611.6, 3118.1, 3129.4, 3195.5, 3224.9, 3741.2
TS6[g]	572.7 i, 214.4, 250.2, 382.7, 461.3, 707.4, 832.4, 942.9, 1009.0, 1118.1, 1273.5, 1364.6, 1437.8, 1499.6, 1560.4, 2344.4, 2967.3, 3014.0, 3048.9, 3074.3, 3807.0
TS7[h]	1828.4 i, 128.1, 198.0, 528.9, 638.6, 879.9, 903.3, 1068.1, 1252.0, 1379.2, 1383.2, 1491.2, 1532.5, 1594.7, 1701.8, 2081.8, 2965.6, 3021.4, 3135.5, 3206.0, 3286.8
TS8[i]	1359.6 i, 130.6, 202.1, 477.3, 551.3, 820.3, 833.3, 1010.7, 1086.8, 1197.4, 1235.5, 1245.0, 1407.4, 1465.8, 1488.8, 1492.6, 3004.2, 3067.1, 3076.4, 3103.7, 3151.3

[a] Calculated at the CASSCF(10,10)/6-311+G** level. [b] $C_2H_5OH \rightarrow H_2C{=}CHOH + H_2$. [c] $C_2H_5OH \rightarrow CH_3CH{=}O + H_2$. [d] $C_2H_5OH \rightarrow CHCH_2OH + H_2$. [e] $C_2H_5OH \rightarrow CH_3COH + H_2$. [f] $C_2H_5OH \rightarrow CH_2{=}CH_2 + H_2O$. [g] $C_2H_5OH \rightarrow CH_3CH + H_2O$. [h] $O(^1D)+C_2H_6 \rightarrow C_2H_5 + OH$ (calculated at the CASSCF(10,10)/6-311+G** level). [i] $O(^3P)+C_2H_6 \rightarrow C_2H_5 + OH$.

TABLE 3: Relative Energy of Molecular Species at the Levels of B3LYP/6-311G(d,p) and CCSD(T)/6-311+G(3df,2p) (in kcal/mol)

species	B3LYP/ 6-311G(d,p) (kcal/mol)[i]	CCSD(T)/ 6-311+G(3df,2p) (kcal/mol)[j]	CCSD(T)/ 6-311+G(3df,2p) + "HLC"[k] (kcal/mol)
$O(^1D)+C_2H_6(D_{3d}\text{-}^1A_{1g})$	0	0	0
$C_2H_5OH(C_s\text{-}^1A')$	−152.8	−142.9	−142.9
$C_2H_5O(C_s\text{-}^2A') + H$	−56.5	−42.7	−39.5
$CH_2CH_2OH(C_1\text{-}^2A) + H$	−54.8	−44.6	−41.4
$C_2H_5(C_s\text{-}^2A') + OH(C_{\infty v}\text{-}^2A_1)$	−66.3	−52.4	−49.2
$CH_3CHOH(C_1\text{-}^2A) + H$	−63.0	−51.6	−48.4
$H_2COH(C_s\text{-}^2A') + CH_3(D_{3h}\text{-}^2A'_1)$	−73.7	−59.6	−56.4
$CH_3CH(C_1\text{-}^1A)-H_2O(C_{2v}\text{-}^1A_1)$ complex	−74.6	−61.7	−61.7
$CHCH_2OH(C_1\text{-}^1A) + H_2(D_{\infty h}\text{-}^1\Sigma^+_g)$	−45.6	−36.1	−36.1
$CH_3COH(C_s\text{-}^1A') + H_2(D_{\infty h}\text{-}^1\Sigma^+_g)$	−90.3	−79.2	−79.2
$H_2C{=}CHOH(C_s\text{-}^1A') + H_2(D_{\infty h}\text{-}^1\Sigma^+_g)$	−130.3	−118.6	−118.6
$CH_3CH{=}O(C_s\text{-}^1A') + H_2(D_{\infty h}\text{-}^1\Sigma^+_g)$	−141.8	−129.8	−129.8
$CH_2{=}CH_2(D_{2h}\text{-}^1A_g) + H_2O(C_{2v}\text{-}^1A_1)$	−140.7	−132.6	−132.6
$CH_3CH(C_1\text{-}^1A)+ H_2O(C_{2v}\text{-}^1A_1)$	−66.7	−59.1	−59.1
$O-C_2H_6(C_s\text{-}^1A'')$			−8.3[l]
TS1[a]	−51.4	−38.2	−38.2
TS2[b]	−69.0	−56.9	−56.9
TS3[c]	−44.8	−34.9	−34.9
TS4[d]	−70.8	−56.9	−56.9
TS5[e]	−89.9	−75.9	−75.8
TS6[f]	−75.0	−61.0	−61.0
TS7[g]			−6.1[l]
TS8[h]		−39.7	−39.7

[a] $C_2H_5OH \rightarrow H_2C{=}CHOH + H_2$. [b] $C_2H_5OH \rightarrow CH_3CH{=}O + H_2$. [c] $C_2H_5OH \rightarrow CHCH_2OH + H_2$. [d] $C_2H_5OH \rightarrow CH_3COH + H_2$. [e] $C_2H_5OH \rightarrow CH_2{=}CH_2 + H_2O$. [f] $C_2H_5OH \rightarrow CH_3CH + H_2O$. [g] $O(^1D)+C_2H_6 \rightarrow C_2H_5 + OH$. [h] $O(^3P)+C_2H_6 \rightarrow C_2H_5 + OH$. [i] Zero-point energy is included in the reported energy values. [j] Single-point calculation using B3LYP/6-311G(d,p) optimized structures. Zero-point energy is included in the reported energy values. See text for detailed description. [k] Higher level correction (HLC) is $-5.25n_\beta - 0.19n_\alpha$, in mhartree. See ref 38 for detailed description. [l] Calculated at the MRCI+Q(8,8)/cc-pvtz/CASSCF(10,10)/6-311+G** level with ZPE obtained at CASSCF(10,10)/6-311+G**.

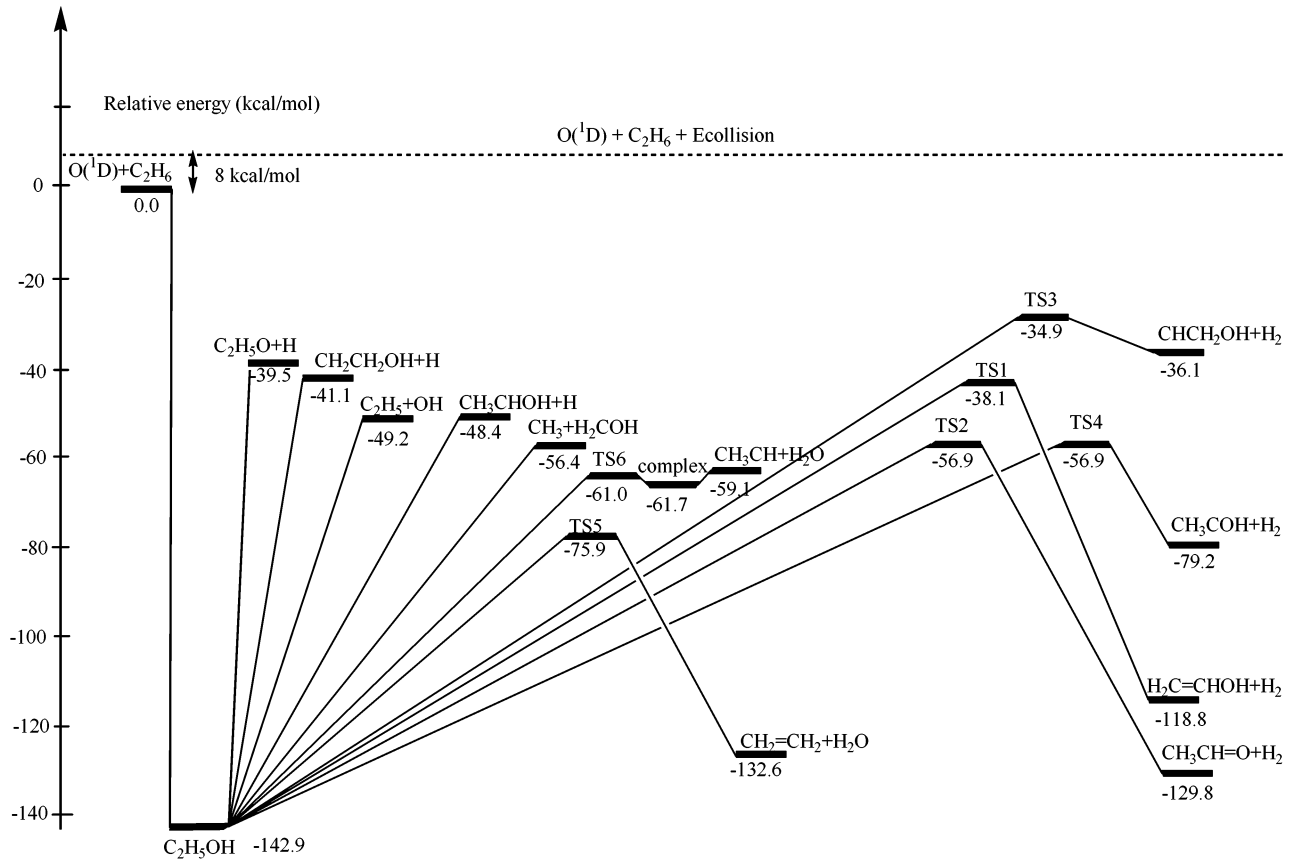

Figure 2. Ground-state potential energy surface of the reaction channels considered in the present calculation. Transition states are marked with TS. See text for detailed description. The energy values shown include the zero-point energy.

input to find the number of states, $W(E - E^{\neq})$, at this C−C bond distance. With this computational procedure, the $W(E - E^{\neq})$ value at every C−C bond distance increasing by 0.1 Å was calculated until a minimal $W(E - E^{\neq})$ was found. A scan

TABLE 4: Bond Length, Relative Energy, and Vibrational Frequencies of Transition State (TS) Obtained Using Microcanonical Variational Transition-State Theory (MVTST) for Bond-Breaking, Barrierless Reaction Channels

species	bond length (in Å)	relative energy (in kcal/mol)[a] B3LYP/ 6-311G(d,p)	relative energy (in kcal/mol)[a] CCSD/ 6-311+G(3df,2p)	vibrational frequency (in cm^{-1})
CH_2CH_2OH-H	2.5	−52.9	−54.4	335.9, 382.1, 393.7, 553.8, 635.5, 810.8, 902.5, 974.0, 1072.7, 1101.6, 1271.7, 1350.5, 1390.4, 1479.2, 1511.5, 3051.0, 3132.0, 3157.7, 3266.1, 3815.9
$CH_3CHOH-H$	2.7	−62.9	−59.5	204.3, 429.2, 450.8, 486.0, 538.8, 712.0, 943.8, 1024.7, 1078.2, 1274.6, 1319.6, 1396.2, 1451.9, 1477.6, 1520.9, 2964.0, 3091.1, 3153.7, 3223.3, 3806.6
C_2H_5O-H	2.2	−58.0	−47.5	259.0, 309.8, 363.1, 430.3, 820.7, 901.1, 945.4, 1126.2, 1132.4, 1265.2, 1326.5, 1388.8, 1472.3, 1503.3, 1539.8, 2953.9, 2992.9, 3041.2, 3116.2, 3128.3
C_2H_5-OH	2.7	−68.9	−57.6	85.1, 162.4, 178.0, 446.1, 641.6, 794.3, 821.3, 1008.8, 1108.7, 1208.3, 1380.4, 1443.3, 1474.9, 1504.1, 2938.7, 3082.7, 3136.1, 3170.0, 3276.4, 3769.3
CH_3-H_2COH	2.8	−76.8	−68.5	43.8, 223.1, 372.4, 508.3, 540.5, 643.3, 801.5, 864.0, 1090.8, 1218.2, 1388.7, 1421.0, 1424.8, 1511.5, 3094.1, 3140.5, 3247.9, 3254.6, 3277.5, 3830.1

[a] Zero point energy is included in the reported energy values.

TABLE 5: Calculated Microcanonical Rate Constants (in s^{-1})

reaction	rate constant
(k_1) $C_2H_5OH \rightarrow H_2C{=}CHOH + H_2$	2.66×10^7
(k_2) $C_2H_5OH \rightarrow CH_3CH{=}O + H_2$	4.32×10^8
(k_3) $C_2H_5OH \rightarrow CHCH_2OH + H_2$	4.06×10^8
(k_4) $C_2H_5OH \rightarrow CH_3COH + H_2$	4.18×10^8
(k_5) $C_2H_5OH \rightarrow CH_2CH_2OH + H$	1.68×10^9
(k_6) $C_2H_5OH \rightarrow CH_3CHOH + H$	5.40×10^9
(k_7) $C_2H_5OH \rightarrow C_2H_5O + H$	1.50×10^8
(k_8) $C_2H_5OH \rightarrow C_2H_5 + OH$	1.30×10^{10}
(k_9) $C_2H_5OH \rightarrow CH_3 + H_2COH$	9.91×10^{10}
(k_{10}) $C_2H_5OH \rightarrow CH_2{=}CH_2 + H_2O$	3.84×10^{10}
(k_{11}) $C_2H_5OH \rightarrow CH_3CH + H_2O$	5.75×10^9

with a grid size smaller than 0.1 Å showed no significant change in the number of states, $W(E - E^{\neq})$. For this C−C bond-breaking case, a minimum $W(E - E^{\neq})$ at 2.8 Å was obtained, listed in the last row of the second column in Table 4. This optimized structure was assumed to be the TS of this C−C bond-breaking reaction channel based on the MVTST method described above. A single-point calculation at the CCSD(T)/6-311+G(3df,2p) level was then carried out for this TS structure to obtain a more accurate energy. This energy and the vibrational frequencies obtained using the B3LYP/6-311G(d,p) level were used to find the final $W(E - E^{\neq})$ in order to calculate the rate constant in eq 2 for this bond-breaking reaction channel. Bond distances, relative energies, and vibrational frequencies of TS structures found using the procedure described above for other bond-breaking reaction channels are listed in Table 5.

It should be noted here that vibrational anharmonicity, which may be important for some reaction channels, is not included in the present calculation. To our knowledge, it is not straightforward to incorporate anharmonicity in the calculations of the number and density of states. However, the present calculated results show that the calculation based on a harmonic approximation gave results that are in good agreement with available experimental data on the product branching ratio of this reaction of $O + C_2H_6$. As with the vibrational anharmonicity, the tunneling effect also is not taken into account in the present rate constant calculations.

III. Results and Discussion

a. Calculated Product Branching Ratio. The calculated rate constants of all primary reactions are listed in Table 5. Using these values, we solved kinetic equations and found product branching ratios of 60, 8, 4, 1, and 27% for the CH_3, OH, H, H_2, and H_2O formation channels; they are listed in Table 6. The first four numbers are in good agreement with the available experimental results of 70, 25, 3, and 2%, while the experimental result for H_2O is not available. It is noted that the calculation underestimates the branching ratio for the OH formation channel (see discussion below). The first three reaction channels break the C−C, C−O, and C−H (or O−H) bonds to form CH_3, OH, and H radicals, respectively. The result of a much smaller amount of H production compared with the first two products is similar to the case of $O + CH_4$, observed in the molecular beam experiments,[7,9] in which the H, H_2, and CH_3 formation channels constitute 5, 18, and 77% of the total reaction, respectively. To explain the product branching ratio that was obtained, we look at the bond dissociation energy for each bond-breaking elementary reaction and corresponding bond strengths. It can be seen in Figure 2 that the calculations give the bond dissociation energies of 86.5, 93.7, and 99.9 kcal/mol for the CH_3, OH, and H formation channels, respectively. The 99.9 kcal/mol value is obtained by averaging over three primary H formation channels and is shown in Figure 2. These values are in good agreement with a quantum chemistry G2 calculation[15] and correlate well with the typical bond strengths of 83, 86, and 98 kcal/mol for the C−C, C−O, and C−H bonds, respectively.[40] The calculated product branching ratios for these three bond-breaking channels correlate well with their corresponding bond strength qualitatively, although a direct quantitative correlation is not straightforward. On the basis of these results and the above discussion for these bond-breaking reaction channels, the order of reaction rates for these reaction channels can be determined qualitatively according to their corresponding bond strengths or dissociation energies. Quantitatively, the energies of the reacting species and their vibrational frequencies need to be found in order to determine the rate constant k in eq 2. For the H_2 formation channel, the result of calculated high-energy barriers, and the resulting low product percentage to form H_2 molecules compared with other reaction channels, as shown in Figure 2, is consistent with the experimental result[20,21] of low percentage for the H_2 formation channel. The present calculated results show good accuracy in finding the product

TABLE 6: Comparison of Calculated Product Branching Ratio with the Available Experimental Data[20,21]

product	theoretical results (%)	experimental results[a] (%)
H	4	2
H_2	1	3
OH	8	25
CH_3	60	70
H_2O	27	

[a] References 20 and 21.

branching ratio for these reaction channels when compared with available experimental data.

b. Significant Amount of Water Formed. In addition to the four reaction channels discussed above, the calculations gave 27% for the H_2O formation channel, which was not detected in the experiments due to a high background signal for water molecules in the apparatus.[20,21] The computation gave a low barrier of 67.0 kcal/mol for the H_2O formation channel when compared with other reaction channels. The large calculated branching ratio for the H_2O formation channel suggests that H_2O is an important minor product of the $O(^1D) + C_2H_6$ reaction. As seen in Figure 2, the H_2O formation comes mainly from combination of the OH group plus a β H on the neighbor C atom, instead of an α H atom due to the much lower energy barrier for the former H_2O formation channel. The contribution from the OH plus an α H is not significant. This result suggests that the $O(^1D) + CH_4$ reaction should not give a significant amount of water in the molecular beam collision-free environment. While the water molecule is difficult to detect using the current experimental apparatus, the present calculated results suggest that the amount of water in the reaction of $O(^1D) + C_2H_6$ should be much larger than that in the $O(^1D) + CH_4$ reaction. This provides a test for observing water molecules in $O(^1D)$ + alkane reactions, which can be verified in future experiments. The present calculated results suggest that when an oxygen atom collides with an alkane derivatives having a β H on the neighboring C atom, a significant amount of water molecules can form in the molecular beam collision-free environment.

c. Physical Basis for Calculated Product Branching Ratio: Energies and Vibrational Frequencies. As described above, the product branching ratios for the bond-breaking cases correlate well qualitatively with the bond strengths or the bond dissociation energies. It is interesting that, as one can see in Figure 2, the TS energy for the H_2O formation channel is lower than the dissociation energy of $CH_3 + CH_2OH$, but the product ratio for the CH_3 channel is larger than that for the H_2O formation channel. The reaction rate of the CH_3 formation channel was found by carrying out a variational RRKM calculation for the bond-breaking, no-energy-barrier reaction channel. Electronic ground state and vibrational frequencies of the calculated species along the bond-breaking coordinate at the selected grid points are needed as input to find the RRKM rate constants. The minimum rate constant was considered to be the rate constant for this reaction. This point is considered to be the TS point for this reaction channel, as described in section II. For this CH_3 formation channel, it was found that this structure is located at a distance of 2.8 Å between the two C atoms. At this point, the ground-state energy is 9.8 kcal/mol higher than the energy of the TS for the H_2O formation channel. Thus, the larger product ratio for the CH_3 formation channel than for the H_2O formation channel is not because of the energy barrier heights of these two reaction channels, but rather due to the vibrational contribution. It is noted that, at the TS point for the CH_3 formation channel, one very low frequency of 43.8 cm^{-1} was found in the frequency calculation. This arises from the fact that, as the C−C bond lengthens, the bond energy weakens. The potential energy curve along this vibrational coordinate turns flatter, resulting in a pseudorotational-like vibration of very low frequency. Because of the existence of this low frequency in the CH_3 formation channel, which results in a much larger number of states $W(E - E^{\neq})$ at the TS point in eq 2, the reaction constant for this channel increases significantly so that this vibrational contribution dominates the contribution of the energy barrier heights. Also, for the OH formation channel of breaking a C−O bond, a low frequency of 85.1 cm^{-1} was found as well. Similar to the C−C bond-breaking case, the existence of the low-frequency vibrational mode should be responsible for the significant amount of the OH radical formed that was obtained through the insertion mechanism. In addition, for the bond-breaking cases of C−H and O−H bonds producing a H radical, the lowest frequency found in the vibration calculation for the H formation channel was 204 cm^{-1}, which is due to the light mass of hydrogen. Unlike the case of breaking C−C and C−O bonds, the amount of H radical formed is not significant because of the relatively high frequencies. These calculated results of vibrational frequencies for the C−C, C−O, and C−H (O−H) bond-breaking cases for determining the rate constants of these reaction channels are likely to be found as well for the reactions of $O(^1D)$ + other larger alkane molecules.

d. Contribution of OH Radical Product via Abstraction Mechanism Is Not Negligible. Among all calculated product branching ratios of the reaction channels examined, the deviation of the calculated result of 8% from the experimental result of 25% for the OH formation channel is significantly larger than for other reaction channels. Even when the H_2O formation percentage is included in a calibration for the experimental results based on the calculated results, the deviation of the calculated value from the experiment for the OH formation channel is still large compared with other reaction channels. This indicates that the abstraction mechanism which produces the OH radical also can contribute to the total reaction. Since the ^1D electronic state of the oxygen atom is 5-fold degenerate, when $O(^1D)$ and C_2H_6 approach each other the potential energy surface splits. The ground-state $^1A'$ surface corresponds to the barrier-less insertion mechanism, leading to an ethanol molecule with an energy gain of ~143 kcal/mol. On the other hand, the first excited $^1A''$ surface also appeared to exhibit an attractive character. The excited open-shell singlet $^1A''$ electronic state cannot be properly treated at the B3LYP or CCSD(T) levels of theory. Therefore, to investigate stationary points on the $^1A''$ potential energy surface, we employed the multireference complete active space self-consistent field (CASSCF) method[41] with the 6-311+G** basis set for geometry optimization and calculations of vibrational frequencies and the internally contracted multireference configuration interaction (MRCI) method[42] with Dunning's correlation-consistent cc-pvtz basis set[43] to refine the single-point energies at the CASSCF optimized geometries. The active space for CASSCF calculations included 10 electrons distributed on 10 orbitals ($5A' + 5A''$) and that for MRCI included 8 electrons on 8 orbitals ($4A' + 4A''$). ZPE corrections were taken from the CASSCF/6-311+G** calculations. MOLPRO 2000[44] and DALTON[45] program packages were used for the multireference calculations. The computed energy profile of the $^1A''$ potential energy surface is shown in Figure 3, and the optimized geometries for two stationary structures are depicted in Figure 4. One can see that $O(^1D)$ and C_2H_6 can form an $O-C_2H_6$ complex in the $^1A''$ electronic state bound by 8.3 kcal/mol relative to the reactants. From the complex, the reaction proceeds by the abstraction mechanism to the $C_2H_5 + OH(^2\Pi)$ products via TS7. The calculated barrier is only 2.2 kcal/mol, so the transition state lies 6.1 kcal/mol below the reactants. This result indicates that the abstraction mechanism is feasible. This mechanism is expected to significantly contribute to the OH formation channel and to account for the forward scattering of this product in the crossed molecular beam experiment. A similar role of the abstraction mechanism

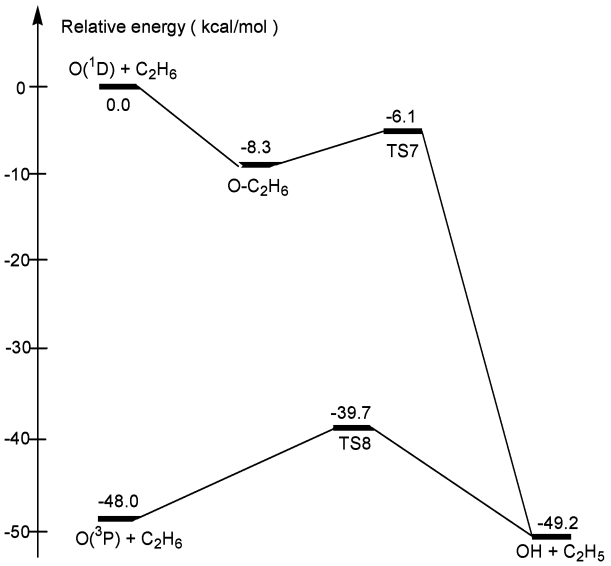

Figure 3. Energy profile of the $O + C_2H_6$ reaction via the abstraction mechanism.

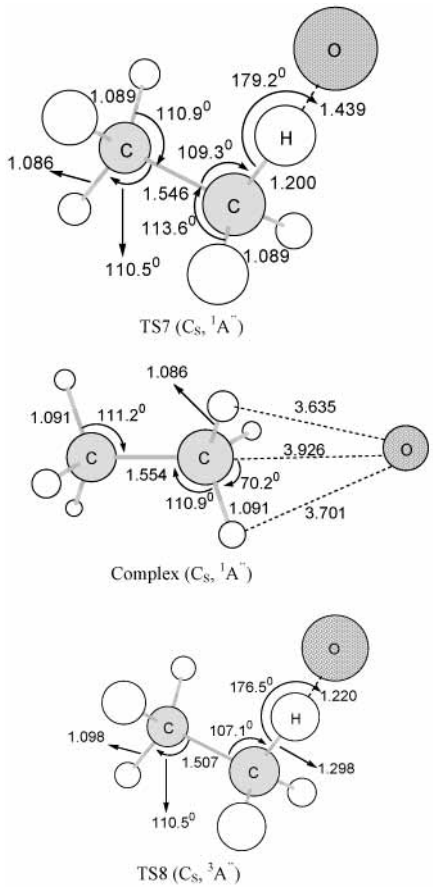

Figure 4. (a) Transition state (TS7) and $O(^1D)-C_2H_6$ complex structures of the $O(^1D) + C_2H_6$ reaction via the abstraction mechanism, obtained at the CASSCF(10,10)/6-311+G** level. (b) Transition state (TS8) structure of the $O(^3P) + C_2H_6$ reaction via the abstraction mechanism, obtained at the B3LYP/6-311G(d,p) level.

involving the first excited $^1A''$ potential energy surface was found earlier for the $O(^1D) + SiH_4$ reaction[46] and is expected to be a common feature of the $O(^1D)$ reactions with saturated hydrids.

In addition to abstraction by $O(^1D)$ atoms, a calculation for $O(^3P)$ was carried out to examine a possible contribution via the abstraction mechanism by $O(^3P) + C_2H_6$. The calculated energies and structures are shown in Figures 3 and 4, respectively. The calculation gave a barrier of 8.3 kcal/mol, higher than the $O + C_2H_6$ collision energy of 8 kcal/mol used in experiment. Thus, formation of OH product via the abstraction mechanism of $O(^3P) + C_2H_6$ is negligible. In any case, quantitative determination of the contribution to forming the OH product via the abstraction mechanism requires an accurate scattering calculation for this reaction along two attractive singlet PES correlated to $O(^1D) + C_2H_6$, which is not included in the present study. Nevertheless, the insertion mechanism is the dominant reaction pathway, although the abstraction mechanism has a non-negligible contribution in producing the OH radical. According to the above calculated results for the abstraction mechanism and this argument, it is suggested that the underestimated calculated branching ratio of 8% for the OH formation channel, which is much lower than the experimental value of 25%, can be compensated by the contribution from the abstraction mechanism of the $O(^1D) + C_2H_6$ collision reaction. The result of the low energy barrier for the abstraction mechanism to produce OH radicals supports a non-negligible contribution of the abstraction mechanism to produce OH radicals. Together with the calculated results discussed above, the present calculations gave theoretical data to help further understand the $O(^1D) + C_2H_6$ reaction. The present results, calculated using a high-level quantum chemistry calculation combined with the RRKM theory, should be of aid in illustrating the reaction kinetics of $O +$ simple alkane molecules in the molecular beam collision-free environment.

IV. Concluding Remarks

In summary, the combined quantum chemistry and RRKM calculation was performed to examine the reaction of $O(^1D) + C_2H_6$ in the molecular beam collision-free environment. The calculated results are in good agreement with available experimental results of the product branching ratio for the CH_3, OH, H, and H_2 formation channels. The calculation also predicts that the $O(^1D) + C_2H_6$ reaction produces water molecules, taking 27% in the total reaction channels in the molecular beam collision-free environment. Additionally, the calculation for OH formation through the abstraction mechanism shows that this channel can contribute significantly to the formation of an OH fragment and compensate for the underestimated, insertion-considered-only percentage of the calculated results compared with the larger experimental result. The present combined quantum chemistry and RRKM calculation shows good accuracy in examining the $O(^1D) + C_2H_6$ reaction in the molecular beam collision-free environment. Previous combined quantum chemistry and RRKM studies of other chemical reactions, for example, photodissociation of the propargyl radical,[47] carbonyl cyanide,[48] 1,2- and 1,3-butadienes,[49] and the $O(^1D) + C_3H_6$ reaction,[50] demonstrated that this method is able to provide product branching ratios with accuracy within 5% as compared to the experiment for the reaction channels occurring on the ground-state potential energy surface. Therefore, the formation of a significant amount of water in the $O(^1D) + C_2H_6$ reaction in the molecular beam collision-free environment is likely to be a reliable prediction and may be verified in a future experiment. The water molecules come from the OH of the activated ethanol plus a β H on the neighboring C atom. This finding suggests that, for the reaction of $O(^1D) + C_3H_8$, the water molecule formation channel should take a non-negligible percentage of the total reaction channels as well. Calculations for the $O(^1D) + C_3H_8$ reaction are currently underway and will be reported in the future.

Acknowledgment. The authors thank Dr. Jim J. Lin for helpful discussion. This research is supported by the National Science Council of Taiwan. Many of the computations in this report were carried out on NCHC computers.

References and Notes

(1) Yamabe, T.; Koizumi, M.; Yamashita, K.; Tachibana, A. *J. Am. Chem. Soc.* **1984**, *106*, 2255.
(2) Rudich, Y.; Hurwitz, Y.; Frost, G. J.; Vaida, V.; Naaman, R. *J. Chem. Phys.* **1993**, *99*, 4500.
(3) Butkovskaya, N. I.; Zhao, Y.; Setser, D. W. *J. Phys. Chem. A* **1994**, *98*, 10779.
(4) Hsu, C. C.; Mebel, A. M.; Lin, M. C. *J. Chem. Phys.* **1996**, *105*, 2346.
(5) Chang, A. H. H.; Mebel, A. M.; Yang, X.; Lin, S. H.; Lee, Y. T. *J. Chem. Phys.* **1998**, *109*, 2748.
(6) Chang, A. H. H.; Mebel, A. M.; Yang, X.; Lin, S. H.; Lee, Y. T. *Chem. Phys. Lett.* **1998**, *287*, 301.
(7) Lin, J. J.; Lee, Y. T.; Yang, X. *J. Chem. Phys.* **1998**, *109*, 2975.
(8) Kaiser, R. I.; Mebel, A. M.; Chang, A. H. H.; Lin, S. H.; Lee, Y. T. *J. Chem. Phys.* **1999**, *110*, 103.
(9) Lin, J. J.; Harich, S.; Lee, Y. T.; Yang, X. *J. Chem. Phys.* **1999**, *110*, 10821.
(10) Liu, X.; Lin, J. J.; Harich, S.; Schatz, G. C.; Yang, X. *Science* **2000**, *289*, 1536.
(11) Dixon, R. N.; Hwang, D. W.; Yang, X. F.; Harich, S.; Lin, J. J.; Yang, X. *Science* **1999**, *285*, 1249.
(12) Kaiser, R. I.; Stranges, D.; Lee, Y. T.; Suits, A. G. *J. Chem. Phys.* **1996**, *105*, 8721.
(13) van Zee, R. D.; Stephenson, J. C. *J. Chem. Phys.* **1995**, *102*, 6946.
(14) Jursic, B. S. *J. Mol. Struct. (THEOCHEM)* **1998**, *422*, 253.
(15) Pople, J. A.; Lucas, D. J.; Curtiss, L. A. *J. Chem. Phys.* **1995**, *102*, 3292.
(16) Jursic, B. S. *J. Mol. Struct. (THEOCHEM)* **2000**, *499*, 91.
(17) Shu, J.; Lin, J. J.; Lee, Y. T.; Yang, X. *J. Chem. Phys.* **2000**, *113*, 96785.
(18) Fernandez, A.; Fontijn, A. *J. Phys. Chem. A* **2001**, *105*, 8196.
(19) Kono, M.; Matsumi, Y. *J. Phys. Chem. A* **2001**, *105*, 65.
(20) Shu, J.; Lin, J. J.; Lee, Y. T.; Yang, X. *J. Chem. Phys.* **2001**, *115*, 849.
(21) Shu, J.; Lin, J. J.; Lee, Y. T.; Yang, X. *J. Chem. Phys.* **2001**, *114*, 4.
(22) Alagia, M.; Balucani, N.; Casavecchia, P.; Lagana, A.; deAspuru, G. O.; Van Kleef, E. H.; Volpi, G. G.; Lendvay, G. *Chem. Phys. Lett.* **1996**, *258*, 323.
(23) Hsu, Y. T.; Wang, J. H.; Liu, K. *J. Chem. Phys.* **1997**, *107*, 1664.
(24) Kurosaki, Y.; Takayanagi, T. *Chem. Phys. Lett.* **2002**, *355*, 424.
(25) Tsang, W. *Int. J. Chem. Kinet.* **1976**, *8*, 173.
(26) Choudhury, T. K.; Lin, M. C.; Lin, C. Y.; Sanders, W. A. *Combust. Sci. Technol.* **1990**, *71*, 219.
(27) Marinov, N. M. *Int. J. Chem. Kinet.* **1999**, *31*, 183.
(28) Xia, W. S.; Zhu, R. S.; Lin, M. C.; Mebel, A. M. *Faraday Discuss.* **2001**, *119*, 191.
(29) Chang, A. H. H.; Lin, S. H. *Chem. Phys. Lett.* **2002**, *363*, 175.
(30) Nguyen, T. L.; Mebel, A. M.; Lin, H. S.; Kaiser, R. I. *J. Chem. Phys.* **2001**, *110*, 10330.
(31) Shu, J.; Lin, J. J.; Wang, C. C.; Lee, Y. T.; Yang, X.; Nguyen, T. L.; Mebel, A. M. *J. Chem. Phys.* **2001**, *115*, 7.
(32) Park, J.; Zhu, R. S.; Lin, M. C. *J. Chem. Phys.* **2002**, *117*, 3224.
(33) Eyring, H.; Lin, H. S.; Lin, S. M. *Basic Chemical Kinetics*; Wiley: New York, 1980.
(34) Garrett, B. C.; Truhlar, D. G. *J. Chem. Phys.* **1979**, *70*, 1593.
(35) Lu, D. H.; Truhlar, D. G. *J. Chem. Phys.* **1993**, *99*, 2723.
(36) Jackels, C. F.; Gu, Z.; Truhlar, D. G. *J. Chem. Phys.* **1995**, *102*, 3188.
(37) Frisch, M. J.; Trucks, G. W.; Schlegel, H. B.; Scuseria, G. E.; Robb, M. A.; Cheeseman, J. R.; Zakrzewski, V. G.; Montgomery, J. A., Jr.; Stratmann, R. E.; Burant, J. C.; Dapprich, S.; Millam, J. M.; Daniels, A. D.; Kudin, K. N.; Strain, M. C.; Farkas, O.; Tomasi, J.; Barone, V.; Cossi, M.; Cammi, R.; Mennucci, B.; Pomelli, C.; Adamo, C.; Clifford, S.; Ochterski, J.; Petersson, G. A.; Ayala, P. Y.; Cui, Q.; Morokuma, K.; Malick, D. K.; Rabuck, A. D.; Raghavachari, K.; Foresman, J. B.; Cioslowski, J.; Ortiz, J. V.; Baboul, A. G.; Stefanov, B. B.; Liu, G.; Liashenko, A.; Piskorz, P.; Komaromi, I.; Gomperts, R.; Martin, R. L.; Fox, D. J.; Keith, T.; Al-Laham, M. A.; Peng, C. Y.; Nanayakkara, A.; Gonzalez, C.; Challacombe, M.; Gill, P. M. W.; Johnson, B.; Chen, W.; Wong, M. W.; Andres, J. L.; Gonzalez, C.; Head-Gordon, M.; Replogle, E. S.; Pople. J. A. *Gaussian 98*; Gaussian Inc.: Pittsburgh, PA, 1998.
(38) Mebel, A. M.; Morokuma, K.; Lin, M. C. *J. Chem. Phys.* **1995**, *103*, 7414.
(39) (a) Madden, L. K.; Mebel, A. M.; Lin, M. C.; Melius, C. F. *J. Phys. Org. Chem.* **1996**, *9*, 801. (b) Bettinger, H. F.; Schreiner, P. R.; Schleyer, P. v. R.; Schaefer, H. F. *J. Phys. Chem.* **1996**, *100*, 16147. (c) Mebel, A. M.; Lin, M. C.; Chakraborty, D.; Park, J.; Lin, S. H.; Lee, Y. T. *J. Chem. Phys.* **2001**, *114*, 8421.
(40) Shriver, D. F.; Atkins, P. W. *Inorganic Chemistry*, 2nd ed.; Oxford University Press: New York, 1994; Table 2.5.
(41) (a) Werner, H.-J.; Knowles, P. J. *J. Chem. Phys.* **1985**, *82*, 5033. (b) Knowles, P. J.; Werner, H.-J. *Chem. Phys. Lett.* **1985**, *115*, 259.
(42) (a) Werner, H.-J.; Knowles, P. J. *J. Chem. Phys.* **1988**, *89*, 5803. (b) Knowles, P. J.; Werner, H.-J. *Chem. Phys. Lett.* **1988**, *145*, 514.
(43) Dunning, T. H., Jr. *J. Chem. Phys.* **1989**, *90*, 1007.
(44) *MOLPRO* is a package of quantum chemistry programs written by H.-J. Werner and P. J. Knowles, with contributions from J. Almlöf, R. D. Amos, M. J. O. Deegan, S. T. Elbert, C. Hampel, W. Meyer, K. Peterson, R. Pitzer, A. J. Stone, P. R. Taylor, and R. Lindh.
(45) Helgaker, T.; Jensen, H. J. Aa.; Jørgensen, P.; Olsen, J.; Ruud, K.; Ågren, H.; Auer, A. A.; Bak, K. L.; Bakken, V.; Christiansen, O.; Coriani, S.; Dahle, P.; Dalskov, E. K.; Enevoldsen, T.; Fernandez, B.; Hättig, C.; Hald, K.; Halkier, A.; Heiberg, H.; Hettema, H.; Jonsson, D.; Kirpekar, S.; Kobayashi, R.; Koch, H.; Mikkelsen, H. V.; Norman, P.; Packer, M. J.; Pedersen, T. B.; Ruden, T. A.; Sanchez, A.; Saue, T.; Sauer, S. P. A.; Schimmelpfennig, B.; Sylvester-Hvid, K. O.; Taylor, P. R.; Vahtras, O. *DALTON*, a molecular electronic structure program, Release 1.2; 2001.
(46) Nguyen, T. L.; Mebel, A. M.; Lin, S. H. *J. Chem. Phys.* **2001**, *114*, 10816.
(47) Nguyen, T. L.; Mebel, A. M.; Lin, S. H.; Kaiser, R. I. *J. Phys. Chem.* **2001**, *105*, 11549.
(48) Lee, H. Y.; Mebel, A. M.; Lin, S. H. *Int. J. Quantum Chem.* **2002**, *90*, 566.
(49) Lee, H. Y.; Kislov, V. V.; Lin, S. H.; Mebel, A. M.; Neumark, D. M. *Chem. Eur. J.* **2003**, *9*, 726.
(50) Wang, C. C.; Lee, Y. T.; Yang, X.; Nguyen, T. L.; Mebel, A. M. *J. Chem. Phys.* **2002**, *116*, 8292.